NANO LETTERS

pubs.acs.org/NanoLett

Ultrahigh Density Array of Epitaxial Ferroelectric Nanoislands on Conducting Substrates

Youngsuk Kim,[†] Hee Han,[‡] Yunseok Kim,[§] Woo Lee,[∥] Marin Alexe,[§] Sunggi Baik,[‡] and Jin Kon Kim*,[†]

[†]National Creative Research Initiative Center for Block Copolymer Self-Assembly and Department of Chemical Engineering and [‡]Department of Materials Science and Engineering, Pohang University of Science and Technology, Pohang, Kyungbuk 790-784, Korea, [§]Max Planck Institute of Microstructure Physics, D-06120 Halle (Saale), Germany, and [∥]Korea Research Institute of Standards and Science (KRISS), Yuseong, Daejon 305-340, Korea

ABSTRACT An ultrahigh density array of epitaxial $PbTiO_3$ (PTO) nanoislands with uniform size was fabricated on a single-crystalline Nb-doped $SrTiO_3$ (100) substrate over a large area (cm^2 scale) by simple but robust method utilizing polystyrene-*block*-poly(4-vinylpridine) copolymer micelles. Each nanoisland has an average volume of 2.6×10^3 nm^3 (a height of 7 nm and a diameter of 22 nm). Because of uniform nanoislands over a large area, a synchrotron X-ray diffraction experiment was successfully employed to analyze the domain structures of PTO nanoislands. They showed well-defined epitaxy on the substrate, which was also confirmed by high-resolution transmission electron microscopy. All of the nanoislands existing in the entire area showed distinct piezoresponse that confirms the existence of ferroelectricity at this size. The results indicate that the critical size of ferroelectrics could be scaled-down further, thereby much increasing the density of ferroelectric devices.

KEYWORDS $PbTiO_3$, ferroelectrics, nanoislands, piezoresponse, block copolymer micelles.

Ferroelectric materials have gained much attention owing to their unique properties of spontaneous, switchable polarization, piezoelectricity, and pyroelectricity. During the past decades, the ferroelectrics of a thin film have been extensively studied both theoretically[1] and experimentally.[2−4] Although continuous ferroelectric thin film has shown the possibility for various applications such as information storage media[5,6] and infrared cameras,[7] discrete nanostructures, for instance, nanoislands or nanodots, are ideal because the crosstalk effect invoked by the domain movement or thermal diffusion could be inherently excluded.[7−10]

For nanostructured ferroelectric materials, it is important to find the critical size below which ferroelectricity disappears, because this size determines the ultimate areal density of ferroelectric devices. It was theoretically predicted that a nanodisk with a diameter of 3.2 nm could maintain spontaneous polarization.[11] However the fabrication of ferroelectric nanostructure at this size level is extremely difficult. Earlier, continuous thin film was carved into discrete nanostructures with controlled size and shape by using focused-ion beam (FIB).[12] But, the crystal structure of nanoislands could be affected during the etching process. Also, the fabrication of nanoislands in a large area is extremely tedious due to a time-consuming process. To overcome these drawbacks, various approaches[13−16] have been employed. Szafraniak et al.[15] employed chemical solution deposition (CSD) method to fabricate epitaxial, single-crystal $PbZr_xTi_{1-x}O_3$ (PZT) nanoislands. Nanoislands with various sizes (height ranging from 9 to 25 nm and lateral dimension from 20 to 200 nm) were obtained by changing initial precursor film thickness and crystallization temperature. A nanoisland with a relatively large volume ($\sim 1.2 \times 10^6$ nm^3) showed ferroelectric properties. Son et al.[16] fabricated ferroelectric nanoislands with a lateral dimension of 37 nm and a height of 22 nm (thus, a volume of 3×10^4 nm^3) by dip-pen lithography and piezoresponse was observed for this nanoisland.

Although the previous studies provide useful information on the critical size of ferroelectric nanoislands, the experimental results have been obtained based on a single nanoisland (or nanostructure). To eliminate the possible error in estimating the critical size, ferroelectric behavior should be obtained from a very large number (say over 10^{10}) of nanoislands with uniform shape and narrow size distribution. Several research groups have pursued this objective.[17−20] Lee et al.[21] fabricated a high-density array of PZT nanoislands with a diameter of 60 nm and a height of 40 nm (volume of 2.8×10^4 nm^3) using pulsed laser deposition and aluminum oxide mask. The crystal structure was analyzed by X-ray diffraction (XRD) owing to the uniform size of PZT nanoislands over a large area. They also found that each PZT nanoisland worked as a ferroelectric capacitor. Although this result showed successful fabrication of a high-density array

* To whom correspondence should be addressed. E-mail: jkkim@postech.ac.kr. Fax: (+) 82-54-279-8298.

Received for review: 03/8/2010
Published on Web: 05/03/2010

DOI: 10.1021/nl100819d | *Nano Lett.* **2010,** *10,* 2141–2146

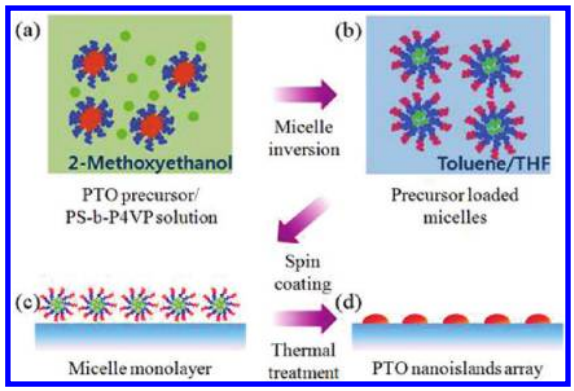

FIGURE 1. Schematic of fabrication of ultrahigh density array of PTO nanoislands on Nb-doped STO(100) substrate. (a) Mixture of the PTO precursor and PS-*b*-P4VP in 2-methoxyethanol. PS block becomes core, whereas P4VP block becomes corona. (b) Micelle inversion and simultaneous incorporation of the PTO precursor into the P4VP core. (c) Monolayer of the precursor-loaded micelles on the substrate by spin coating. (d) Ultrahigh density array of PTO nanoislands over a large area (1 cm^2) after removal of PS-*b*-P4VP and the organic moieties of the PTO precursor.

of ferroelectric nanoislands, the lateral dimension of a nanoisland is still larger than that obtained by self-assembly based on CSD.[15] It is noted, however, that CSD could not produce ferroelectric nanostructures with uniform size. We realize that when ferroelectric nanoislands are prepared by block copolymer micelles,[22−25] the size is comparable to (or smaller than) that obtained by CSD, while maintaining uniform size distribution. Furthermore, the in-plane ordering of the nanoislands on various conducting substrates is good due to the self-assembly of the micelles.

In this study, we prepared an ultrahigh density array of ferroelectric $PbTiO_3$ (PTO) nanoislands on Nb-doped $SrTiO_3$ (STO)(100) substrate by using polystyrene-*block*-poly(4-vinyl pyridine) copolymer (PS-*b*-P4VP) micelles. The fabricated PTO nanoislands had uniform size distribution in a large area (over cm^2 scale), and a good in-plane ordering of the nanoislands was obtained. The average diameter (D) and height (h) of each nanoisland were 22 and 7 nm, respectively. Thus, each nanoisland had a volume of $\sim 2.6 \times 10^3$ nm^3 and a scaling ratio (D/h) of 3.3. Well-developed epitaxy of the PTO nanoislands was successfully analyzed by synchrotron X-ray diffraction (XRD) and transmission electron microscopy (TEM). Piezoresponse of the nanoislands was examined by piezoresponse force microscopy (PFM), and all of the nanoislands existing in the entire area showed distinct ferroelectricity. These observations confirm that the ferroelectricity of PTO nanoislands could be maintained at a volume as small as 2.6×10^3 nm^3 and high scaling ratio of 3.3.

Figure 1 gives a schematic of the preparation of an ultrahigh density array of PTO nanoislands on Nb-doped STO(100) substrate by using PS-*b*-P4VP micelles. First, PS-*b*-P4VP with molecular weights of 41 500 and 17 500 for each block was dissolved into PTO precursor solution diluted with 2-methoxyethanol. We chose PS-*b*-P4VP because of a favorable interaction between the precursor and pyridine ring in the P4VP block, which was confirmed by Fourier-transform infrared (FTIR) spectroscopy (Supporting Information Figure S1a). Since 2-methoxyethanol is a selective solvent of P4VP, the PS block becomes micelle core in 2-methoxyethanol solution and the precursor remains outside the micelle core (Figure 1a). To incorporate PTO precursor into the micelle core, a toluene/tetrahydrofuran mixture (v/v = 3/1) was carefully added to the 2-methoxyethanol solution. Then, the precursor was incorporated into the P4VP cores by micelle inversion (Figure 1b). By controlling the concentration of PS-*b*-P4VP in the solution, a monolayer of the precursor-loaded micelles was prepared on single-crystalline Nb-doped STO(100) substrate by spin coating (Figure 1c). The substrate employed in the present study was chosen by considering the good electrical conductivity and small lattice mismatch between the PTO (a = 3.899 Å)[26] and Nb-doped STO (a = 3.905 Å).[27] To prevent surface reconstruction during crystallization of PTO, the substrate was etched and annealed at 900 °C (Supporting Information Figure S2). Finally, PS-*b*-P4VP and organic moiety of the PTO precursor were simultaneously removed, while the PTO nanoislands became epitaxially crystallized on the substrate by heat treatment at 600 °C for 1 h in air (Figure 1d). Because of the volatility of Pb at this temperature, we used the PTO precursor with a molar ratio of Pb to Ti of 1.1.

Figure 2a,b gives atomic force microscopy (AFM) topography images of the array of the PTO precursor-loaded micelles and the array of the PTO nanoislands after removal of PS-*b*-P4VP and crystallization of the precursor. Figure 2c gives an enlarged AFM topography image of Figure 2b and the height profile along the red line. The average diameter of the precursor-loaded micelles was 60 nm (Figure 2a), which is larger than that (~50 nm) of the pristine micelles (Supporting Information Figure S3). The increase in micelle diameter upon precursor loading can be attributed to the reduction of micellization enthalpy and thus, the increase of the aggregation number per micelle.[28] From Figure 2b,c, the average diameter and the height of PTO nanoislands were obtained as 22 and 7 nm, respectively. From the AFM topography image, the size distribution of the nanoislands is quite narrow (21.9 ± 3.5 nm) (see Supporting Information Figure S4a,c). The narrow size distribution is also consistent with the results obtained from scanning electron microscopy (SEM) (Figure S4b). During the thermal decomposition of PS-*b*-P4VP and the organic moieties of the PTO precursor, the micelles were shrunken largely along the height direction. Thus, the resulting PTO nanoislands have a disklike (pancake) shape. Assuming that the PTO nanoislands have disklike structure, the volume of each nanoisland was calculated as 2.6×10^3 nm^3. The average center-to-center distance (D_o) between two neighboring PTO nanoislands was 63 nm, which is essentially the same as that of micelle array (Figures 2a,b). Quasi-hexagonal packing of as-spun micelles and the PTO nanoislands was observed. This indicates that the original arrangement of the micelles is well maintained

DOI: 10.1021/nl100819d | *Nano Lett.* **2010,** *10,* 2141--2146

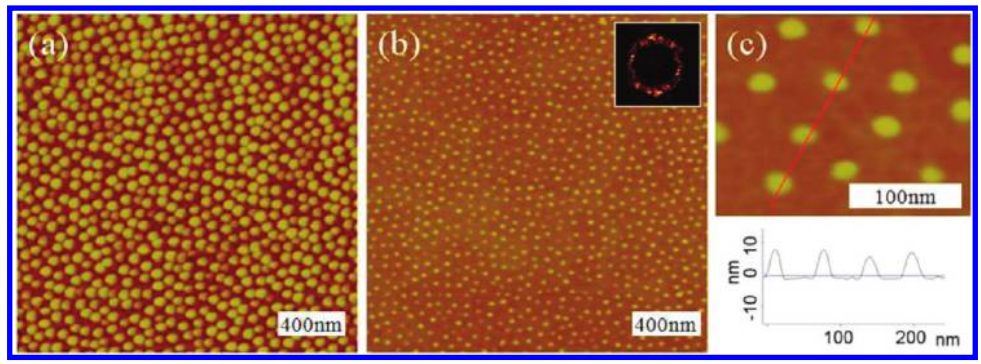

FIGURE 2. AFM topography images of the array of (a) precursor-loaded micelles and (b) the PTO nanoislands after crystallization. Inset shows fast Fourier transform of the image. (c) Enlarged image of part of (b) and the AFM height profile along the red line.

even after the heat treatment at a high temperature for crystallization. Areal density of 297 μm^{-2} (0.18 $Tb \cdot in^{-2}$) was calculated from the number of the PTO nanoislands given in Figure 2b. D_o is determined by the total molecular weight of the block copolymer, and the diameter of the core (which determines the nanoisland size) is proportional to the molecular weight of the core block. With another PS-*b*-P4VP with similar molecular weight of the core block (P4VP) but much shorter corona block (PS) than that in PS-*b*-P4VP employed in this study, the D_o could be significantly decreased without affecting the diameter of a nanoisland. If the thickness of the corona block would be decreased to ~4 nm, while the core diameter is maintained at ~22 nm, D_o would be reduced to ~30 nm. In this situation, an areal density of ~1 $Tb \cdot in^{-2}$ would be obtained.

Because the PTO nanoislands are prepared over a large area, the crystal structure and epitaxial nature of PTO nanoislands grown on Nb-doped STO(100) substrate could be confirmed by synchrotron XRD. Figure 3a shows a $\theta-2\theta$ scan along the normal direction to the substrate. PTO(001) and (002) peaks are clearly observed near Nb-doped STO(001) and (002) peaks, respectively, and no other noticeable crystallographic planes were detected in this range. This result indicates that the PTO nanoislands were grown along (001) orientation. The in-plane epitaxial relationship between the substrate and the PTO nanoislands was investigated by 360° ϕ-scan for (101) diffraction of Nb-doped STO(100) and PTO (Figure 3b). Perfectly overlapped four peaks with 90° separation of PTO and Nb-doped STO(101) peaks manifest the cube-on-cube epitaxial relationship of PTO[100]//STO[100] and PTO(001)//STO(001). The domain structure of the PTO nanoislands was investigated by two-dimensional reciprocal space mapping near the Nb-doped STO(001) reflection (Figure 3c). The contour plot of the *HL*-plane scan clearly shows that the PTO nanoislands consist of only *c*-domain structures without nontilted- or twinned *a*-domains whose *a*-axis are parallel or slightly tilted to the surface normal direction.[21]

This observation is consistent with the previous result that the amount of *c*-domain increases with decreasing height.[29] Namely, with decreasing height the formation of *a*-domain is energetically unfavorable; thus the relaxation of residual strain by *a*-domain is hindered.[30] In addition, strain relaxation by reducing the lateral dimension does not occur due to the high scaling ratio.[29] Also, tetragonality *c*/*a* of 1.060 was calculated from the peak positions of PTO(001) and PTO(101) (see Section S4 in the Supporting Information), which is slightly smaller than that (1.065) of the bulk PTO.[31] Decreased tetragonality indicates that atomic displacement between Ti and O would be also decreased, implying that a reduced spontaneous polarization is expected.[32]

Figure 4a shows a high-resolution transmission electron microscopy (HRTEM) image of the cross-sectional view of a single PTO nanoisland. The PTO nanoisland has a mesalike structure, flattened top surface and slanted sidewalls, whose width and height are 22 and 6 nm, respectively. This shape is consistent with AFM height profile (Figure 2c). The tetragonality of the PTO nanoisland was calculated to be 1.056 based on the lattice spacing shown in Figure 4b), which is almost the same as that obtained from XRD analysis. The epitaxial relation between the PTO nanoisland and the substrate was also confirmed by selected area electron diffraction (SAED) (Figure 4c).

Figure 5a–c gives topography image, PFM phase and PFM amplitude of the PTO nanoislands, respectively. Figure 5a is in accordance with Figure 2b and piezoresponse images (Figure 5b,c), implying that all of the PTO nanoislands are distinctly ferroelectric. All the pristine PTO nanoislands showed preferential upward polarizations; thus they appeared as dark regions in the PFM phase image (Figure 5b). Also, there is no difference in the phase contrast within a single nanoisland, which suggests that no *a*-domain is in existence, coincident with XRD results (Figure 3). The amplitude of the spontaneous polarization of nanoislands is clearly distinguishable from the background, as shown in Figure 5c. Piezoelectric coefficient d_{33} was obtained from a linear plot of amplitude of piezoresponse and applied voltage. Spontaneous polarization (P_S) of the as-grown PTO nanoislands is strongly imprinted and could not be fully switched. Since this could not be explained by the distorted crystal lattices arising from the dislocation at the interface between the PTO nanoislands and the substrate,[33] it might

DOI: 10.1021/nl100819d | *Nano Lett.* **2010,** *10,* 2141–2146

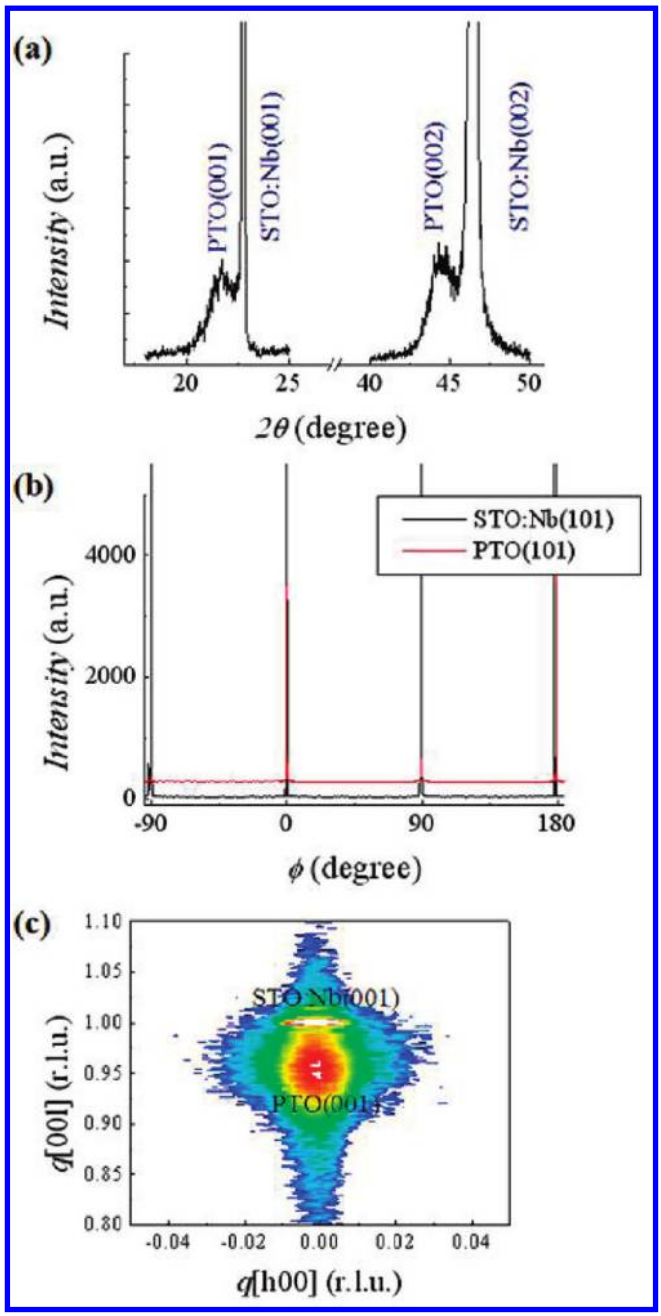

FIGURE 3. (a) $\theta-2\theta$ scan of nanoislands, (b) ϕ scan of PTO(101) and Nb-doped STO(101), (c) *HL* reciprocal space mapping around PTO(001) and Nb-doped STO(001).

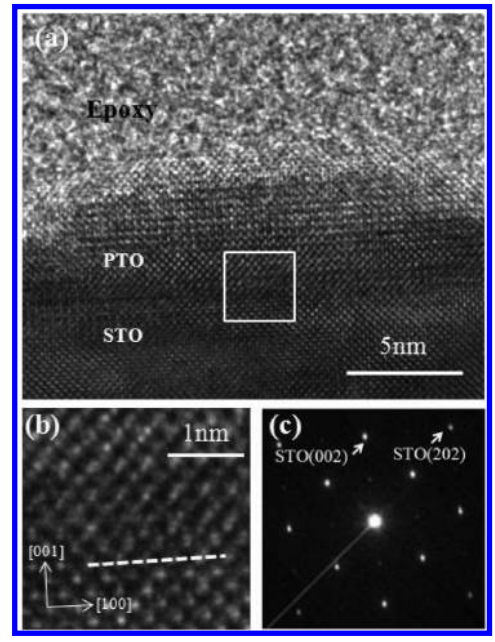

FIGURE 4. (a) A cross-sectional TEM micrograph of PTO/Nb-doped STO(100). (b) An enlarged TEM image of the area marked by a square in (a). The dashed line in (b) indicates the interface between PTO nanoisland (top part) and Nb-doped STO(100) (bottom part). (c) Selected-area electron diffraction (SAED) pattern obtained from the interface.

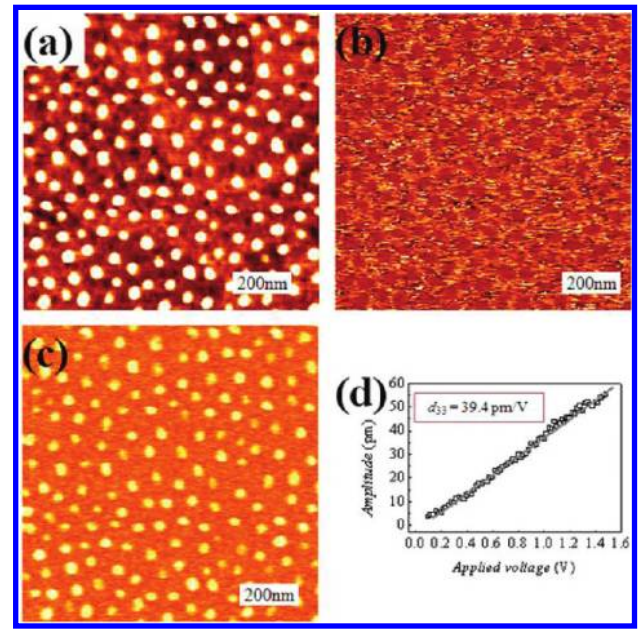

FIGURE 5. (a) Topography, (b) PFM phase, and (c) PFM amplitude images of PTO nanoislands. (d) Amplitude of piezoresponse versus applied voltage graph. The slope of the linear relationship between amplitude and applied voltage gives the piezoelectric coefficient d_{33}.

be attributed to extrinsic effects, such as built-in potentials induced by the trapped space charges at the PTO/Nb-doped STO interface,[34] PbO losses during the thermal treatment, or chemical and/or electronic depletion which usually happens at the surface of Nb-doped STO.[35−37] Nevertheless, the value of d_{33} (39.4 pm/V) of each PTO nanoisland was marked (Figure 5d). Smaller value of d_{33} than that (∼75 pm/V) of the bulk PTO is consistent with reduced tetragonality measured by XRD and HRTEM.

The piezoresponse of PTO nanoislands depends on the size[38] and the scaling ratio.[39,40] The size of nanostructured ferroelectric materials determines the interacting volume, which is proportional to the amplitude of piezoresponse. It is noted that ferroelectricity for a discrete nanostructure decreases with decreasing volume. This is because the Curie temperature of a ferroelectric decreases and even-

DOI: 10.1021/nl100819d | *Nano Lett.* **2010,** *10,* 2141--2146

tually becomes paraelectric at room temperature with decreasing size.[41,42] Roelofs et al. reported that a nanoisland having a volume of 2×10^3 nm^3 did not show piezoresponse, while another nanoisland with a volume of 7.2×10^3 nm^3 showed piezoresponse.[13,43] On the other hand, the scaling ratio estimates the clamping effect of a substrate on the nanostructure; thus, it is inversely proportional to the amplitude of piezoresponse.[39,40] It should be noted that the PTO nanoislands prepared in this study showed considerable piezoresponse even though they have a high scaling ratio (3.3) and a small height (7 nm, about 17 unit cells) and a small volume (2.6×10^3 nm^3). We found that the volume (or the diameter) of nanoislands is directly correlated with piezoresponse amplitude (Supporting Information Figure S4c,d). Also, the size-driven ferroelectric-paraelectric transition did not occur within the size ranges (15−26 nm), implying that the critical size might be smaller than 15 nm (Supporting Information Figure S4d) Although high scaling ratio and small height would impose a severe strain over the PTO nanoislands, a small lateral size (∼22 nm) and *c*-domain abundance may enhance the uniformity of the piezoresponse through the whole nanoislands, resulting in relatively high piezoresponse.

In summary, we have demonstrated that an ultrahigh density array of PTO nanoislands with a lateral dimension of 22 nm and a height of 7 nm was successfully fabricated on Nb-doped STO(100) substrate by using block copolymer micelles followed by epitaxial crystallization. The epitaxial relationship between the PTO nanoislands and the substrate was confirmed by XRD and HRTEM. Nanoislands had good lateral ordering owing to the self-assembly of the micelles. The ultrahigh density PTO nanoislands with narrow size distribution on a large area showed well developed *c*-domains without any noticeable *a*-domains. Even though each of the PTO nanoislands fabricated in this study had a volume as small as 2.6×10^3 nm^3 and a scaling ratio of 3.3, exhibited distinct spontaneous polarization at room temperature. The result suggests that the critical size of ferroelectrics could be scaled-down further, and thus the density of ferroelectric devices would be much increased. Ferroelectric nanoislands with smaller volumes could be also prepared easily by tuning the molecular weight of PS-*b*-P4VP.

Acknowledgment. This work was supported by the National Creative Research Initiative Program of National Research Foundation of Korea (NRF), in part by the second stage of the BK21 program of Korea, the Alexander von Humboldt Foundation, and KRCF through the KRISS project. XRD experiment was performed at PLS beamlines 3C2 and 10C1 supported by POSCO and NRF.

Supporting Information Available. Experimental details, TEM image and FT-IR spectrum of precursor loaded micelles, surface reconstruction of substrate, effect of precursor concentration on micelle size and PTO nanoisland array, size distribution of nanoislands, distribution of piezoresponse of nanoislands, and experimental method to calculate *c*/*a*. This material is available free of charge via the Internet at http://pubs.acs.org.

REFERENCES AND NOTES

(1) Junquera, J.; Ghosez, P. *Nature* **2003**, *422*, 506–509.
(2) Maruyama, T.; Saitoh, M.; Sakai, I.; Hidaka, T.; Yano, Y.; Noguchi, T. *Appl. Phys. Lett.* **1998**, *73*, 3524–2526.
(3) Tybell, T.; Ahn, C. H.; Triscone, J.-M. *Appl. Phys. Lett.* **1999**, *75*, 856–858.
(4) Fong, D. D.; Stephenson, G. B.; Streiffer, S. K.; Eastman, J. A.; Auciello, O.; Fuoss, P. H.; Thompson, C. *Science* **2004**, *304*, 1650–1653.
(5) Gruverman, A.; Auciello, O.; Tokumoto, H. *Annu. Rev. Mater. Sci.* **1998**, *28*, 101–123.
(6) Cho, Y.; Hashimoto, S.; Odagawa, N.; Tanaka, K.; Hiranaga, Y. *Nanotechnology* **2006**, *17*, S137–S141.
(7) Lang, S. B. *Phys. Today* **2005**, *58*, 31–36.
(8) Odagawaa, N.; Cho, Y. *Appl. Phys. Lett.* **2006**, *89*, 192906-1-3.
(9) Würfel, P.; Ruppel, W. *Ferroelectrics* **1989**, *91*, 113–125.
(10) Kohli, M.; Wuethrich, C.; Brooks, K.; Willing, B.; Forster, M.; Muralt, P.; Setter, N.; Ryser, P. *Sens. Actuators, A* **1997**, *60*, 147–153.
(11) Naumov, I. I.; Bellaiche, L.; Fu, H. *Nature* **2004**, *432*, 737–740.
(12) Ganpule, C. S.; Stanishevsky, A.; Su, Q.; Aggarwal, S.; Melngailis, J.; Williams, E.; Ramesh, R. *Appl. Phys. Lett.* **1999**, *75*, 409–411.
(13) Roelofs, A.; Schneller, T.; Szot, K.; Waser, R. *Nanotechnology* **2003**, *14*, 250–253.
(14) Fujisawa, H.; Okaniwa, M.; Nonomura, H.; Shimizu, M.; Niu, H. *J. Eur. Ceram. Soc.* **2004**, *24*, 1641–1645.
(15) Szafraniak, I.; Harnagea, C.; Scholz, R.; Bhattacharyya, S.; Hesse, D.; Alexe, M. *Appl. Phys. Lett.* **2003**, *83*, 2211–2213.
(16) Son, J. Y.; Shin, Y.-H.; Ryu, S.; Kim, H.; Jang, H. M. *J. Am. Chem. Soc.* **2009**, *131*, 14676–14678.
(17) Clemens, S.; Schneller, T.; van der Hart, A.; Peter, F.; Waser, R. *Adv. Mater.* **2005**, *17*, 1357–1361.
(18) Bühlmann, S.; Muralt, P.; Allmen, S. V. *Appl. Phys. Lett.* **2004**, *84*, 2614–2616.
(19) Ma, W.; Hesse, D.; Gösele, U. *Small* **2005**, *1*, 837–841.
(20) Ma, W.; Harnagea, C.; Hesse, D.; Gösele, U. *Appl. Phys. Lett.* **2003**, *83*, 3770–3772.
(21) Lee, W.; Han, H.; Lotnyk, A.; Schubert, M. A.; Senz, S.; Alexe, M.; Hesse, D.; Baik, S.; Gösele, U. *Nat. Nanotechnol.* **2008**, *3*, 402–407.
(22) Förster, S.; Antonietti, M. *Adv. Mater.* **1998**, *10*, 195–217.
(23) Yun, S.-H.; Yoo, S. I.; Jung, J. C.; Zin, W.-C.; Sohn, B.-H. *Chem. Mater.* **2006**, *18*, 5646–5648.
(24) Qi, L.; Cölfen, H.; Antonietti, M. *Nano Lett.* **2001**, *1*, 61–65.
(25) Boyen, H.-G.; Kästle, G.; Zürn, K.; Herzog, T.; Weigel, F.; Ziemann, P.; Mayer, O.; Jerome, C.; Möller, M.; Spatz, J. P.; Garnier, M. G.; Oelhafen, P. *Adv. Funct. Mater.* **2003**, *13*, 359–364.
(26) Lee, K. S.; Baik, S. *J. Appl. Phys.* **1999**, *85*, 1995–1997.
(27) Dubourdieu, C.; Rosina, M.; Audiera, M.; Weissa, F.; Sénateur, J. P.; Dooryhee, E.; Hodeau, J. L. *Thin Solid Films* **2001**, *400*, 81–84.
(28) Xing, L.; Mattice, W. L. *Macromolecules* **1997**, *30*, 1711–1717.
(29) Han, H.; Lee, K.; Lee, W.; Alexe, M.; Hesse, D.; Baik, S. *J. Mater. Sci.* **2009**, *44*, 5167–5181.
(30) Ren, S. B.; Lu, C. J.; Liu, J. S.; Shen, H. M.; Wang, Y. N. *Phys. Rev. B* **1996**, *54*, 14337–14339.
(31) Nelmes, R. J.; Kuhs, W. F. *Solid State Commun.* **1985**, *54*, 721–723.
(32) Lichtensteiger, C.; Triscone, J.-M.; Junquera, J.; Ghosez, P. *Phys. Rev. Lett.* **2005**, *94*, No. 047603-1-4.
(33) Chu, M.-W.; Szafraniak, I.; Scholz, R.; Harnagea, C.; Hesse, D.; Alexe, M.; Gösele, U. *Nat. Mater.* **2004**, *3*, 87–90.
(34) Okatan, M. B.; Alpay, S. P. *Appl. Phys. Lett.* **2009**, *95*, No. 092902-1-3.

DOI: 10.1021/nl100819d | *Nano Lett.* **2010,** *10,* 2141–2146

(35) Rahmati, B.; Fleig, J.; Sigle, W.; Bischoff, E.; Maier, J.; Rühle, M. *Surf. Sci.* **2005**, *595*, 115–126.
(36) Sun, J. R.; Shen, B. G.; Tian, H. F.; Li, J. Q.; Weng, Y. X. *Appl. Phys. Lett.* **2005**, 87.
(37) Menke, T.; Meuffels, P.; Dittmann, R.; Szot, K.; Waser, R. *J. Appl. Phys.* **2009**, *105*, No. 066104-1-3.
(38) Nagarajan, V.; Junquera, J.; He, J. Q.; Jia, C. L.; Waser, R.; Lee, K.; Kim, Y. K.; Baik, S.; Zhao, T.; Ramesh, R.; Ghosez, P.; Rabe, K. M. *J. Appl. Phys.* **2006**, *100*, No. 051609-1-10.
(39) Nagarajan, V. *Appl. Phys. Lett.* **2005**, *87*, No. 242905-1-3.
(40) Lee, K.; Baik, S. *Annu. Rev. Mater. Sci.* **2006**, *36*, 81–116.
(41) Ishikawa, K.; Yoshikawa, K.; Okada, N. *Phys. Rev. B* **1988**, *37*, 5852–5855.
(42) Zhong, W. L.; Wang, Y. G.; Zhang, P. L.; Qu, B. D. *Phys. Rev. B* **1994**, *50*, 698–703.
(43) Rüdiger, A.; Schneller, T.; Roelofs, A.; Tiedke, S.; Schmitz, T.; Waser, R. *Appl. Phys. A* **2005**, *80*, 1247–1255.

DOI: 10.1021/nl100819d | *Nano Lett.* **2010,** *10,* 2141--2146